

Beyond the standard model of topological Josephson junctions: From crystalline anisotropy to finite-size and diode effects

Barış Pekerten ¹, David Brandão ¹, Bailey Bussiere ¹, David Monroe ¹, Tong Zhou ^{1,2}, Jong E. Han ¹, Javad Shabani ³, Alex Matos-Abiague,⁴ and Igor Žutić ¹

¹*Department of Physics, University at Buffalo, State University of New York, Buffalo, New York 14260, USA*

²*Eastern Institute for Advanced Study, Eastern Institute of Technology, Ningbo, Zhejiang 315200, China*

³*Center for Quantum Phenomena, Department of Physics, New York University, New York, New York 10003, USA*

⁴*Department of Physics and Astronomy, Wayne State University, Detroit, MI 48201, USA*

(*Corresponding author: zigor@buffalo.edu)

(*Corresponding author: barispek@buffalo.edu)

(Dated: 11 June 2024)

A planar Josephson junction is a versatile platform to realize topological superconductivity over a large parameter space and host Majorana bound states. With a change in Zeeman field, this system undergoes a transition from trivial to topological superconductivity accompanied by a jump in the superconducting phase difference between the two superconductors. A standard model of these Josephson junctions, which can be fabricated to have a nearly perfect interfacial transparency, predicts a simple universal behavior. In that model, at the same value of Zeeman field for the topological transition, there is a π phase jump and a minimum in the critical superconducting current, while applying a controllable phase difference yields a diamond-shaped topological region as a function of that phase difference and a Zeeman field. In contrast, even for a perfect interfacial transparency, we find a much richer and nonuniversal behavior as the width of the superconductor is varied or the Dresselhaus spin-orbit coupling is considered. The Zeeman field for the phase jump, not necessarily π , is different from the value for the minimum critical current, while there is a strong deviation from the diamond-like topological region. These Josephson junctions show a striking example of a nonreciprocal transport and superconducting diode effect, revealing the importance of our findings not only for topological superconductivity and fault-tolerant quantum computing, but also for superconducting spintronics.

Josephson junctions (JJs), with two superconductors (S) separated by a nonsuperconducting (normal) region (N) provide a fascinating manifestation of proximity effects, where a given material is transformed by its neighbors.^{1,2} The superconductivity leaking from the two S regions can merge, establishing a relative phase difference, ϕ , transforming the whole N region into a superconductor.³ Decades before Josephson's prediction,⁴ this behavior was realized experimentally.^{1,5} Even in conventional materials, through proximity effects, JJs reveal an exotic emergent behavior, absent in any of their constituent regions. With the interplay between spin-orbit coupling (SOC) and Zeeman field (applied or due to exchange coupling), the proximity-induced superconductivity could be transformed from a conventional spin-singlet into spin-triplet p -wave superconductivity. This system could support topological superconductivity over an enhanced parameter range by the applied relative phase difference.^{6–12}

After Kitaev's pioneering work on spin-triplet topological superconductivity and Majorana bound states (MBS),^{13,14} an early work suggested planar JJs as materials realization that supports non-Abelian properties.⁶ However, most of the subsequent studies have focused on proximitized semiconductor nanowires^{15–21} and MBS detection through the quantized zero-bias conductance peak,^{22–25} which can also arise from extrinsic effects.^{26–28} Experiments have realized a high-transparency epitaxially grown planar JJs with proximity-induced superconductivity from Al into the InAs two-dimensional electron gas (2DEG).²⁹ This advance has

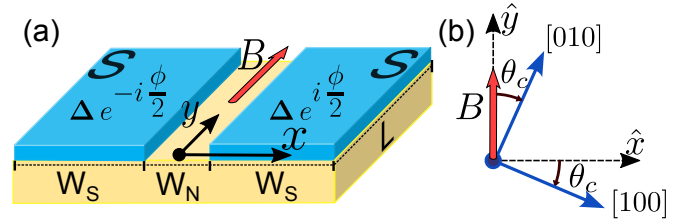


FIG. 1. (a) Planar JJ formed by two superconducting (S) regions with superconducting gap Δ and phase difference ϕ covering a 2DEG normal (N) region. Coordinate axes and JJ dimensions are indicated. The supercurrent I flows along $\pm\hat{x}$, perpendicular to the applied magnetic field \mathbf{B} . (b) The misalignment of the crystallographic direction $[010]$ and \mathbf{B} is represented by the angle θ_c which, with Dresselhaus SOC, leads to crystalline anisotropy.

stimulated important theoretical efforts recognizing that topological superconductivity can be supported over a larger parameter range than in semiconductor nanowires, while also providing phase-sensitive signatures,^{10,11,30} as well other opportunities in 2D platforms.^{12,31–38}

Experiments on planar JJs,^{39–44} including detecting the phase signature of topological superconductivity⁴¹ and a superconducting diode effect,^{41,45–47} reveal a much richer physics than the standard model. Such a model predicts a universal behavior for highly-transparent interfaces, with the diamond-like topological region as a function of ϕ and in-

plane Zeeman field.¹¹ In this work, we provide a more general description of planar JJs for the geometry illustrated in Fig. 1(a), where W_S (W_N) the width of the S (N, uncovered 2DEG) region and L is the length. In Fig. 1(b), the presence of Dresselhaus SOC in the 2DEG^{48,49} and a related crystalline anisotropy is represented by the angle θ_c .⁵⁰⁻⁵² We show that a finite W_S and Dresselhaus SOC each strongly modify the properties of planar JJs implied by the standard model.

We solve the discretized Bogoliubov-de Gennes (BdG) equation using a finite-difference method for BdG Hamiltonian, H_{BdG} , in the Nambu basis $(\psi_\uparrow, \psi_\downarrow, \psi_\downarrow^\dagger, -\psi_\uparrow^\dagger)$ with ψ (ψ^\dagger) destruction (creation) operators of the given spin^{50,52}

$$H_{\text{BdG}} = \left[\frac{\mathbf{p}^2}{2m^*} - \mu(x, y) + H_{\text{SO}} \right] \tau_z - \frac{g^* \mu_B}{2} \mathbf{B} \cdot \boldsymbol{\sigma} + \Delta(x, y) \tau_+ + \Delta^*(x, y) \tau_-, \quad (1)$$

where H_{SO} contains Rashba and Dresselhaus SOC terms

$$H_{\text{SO}} = \frac{\alpha}{\hbar} (p_y \sigma_x - p_x \sigma_y) + \frac{\beta}{\hbar} [(p_x \sigma_x - p_y \sigma_y) \cos 2\theta_c - (p_x \sigma_y + p_y \sigma_x) \sin 2\theta_c]. \quad (2)$$

Here, \mathbf{p} is the momentum, $\mu(x, y)$ is the chemical potential, $\mathbf{B} = B\hat{y}$ is the in-plane magnetic field, μ_B is the Bohr magneton, while m^* and g^* are the effective mass and g -factor. The proximity-induced s -wave superconducting gap term is $\Delta(x, y) = \Delta_0 f_{\text{BCS}}(B, T) \Theta(|x - W_N/2|) \exp[i\phi(x, y)/2]$, where Θ is the step function and $\phi(x, y) = \phi_0 \text{sgn}(x)$, with ϕ_0 the phase difference across the JJ, while Δ_0 is real and uniform in the S regions. The usual BCS dependence of $\Delta(x, y)$ on B and temperature, T , is given by $f_{\text{BCS}}(B, T)$ with $f_{\text{BCS}}(B = 0, T = 0) = 1$.⁵³ α (β) is the Rashba (Dresselhaus) SOC strength. We consider that y direction is translationally invariant in Eq. (1), such that wavevector $k_y = p_y/\hbar$ is a good quantum number, and numerically obtain the energy spectrum and topological properties of its discretized version.^{52,54}

Planar JJs can be phase biased; for example, ϕ can be externally set by embedding a JJ in a superconducting loop threading the magnetic flux through the loop. Alternatively, a phase-unbiased JJ attains its ground state value, ϕ_{GS} , at which the free energy of the system, $F(\phi, B)$, is minimized and satisfies $\partial_\phi F(\phi_{\text{GS}}, B) = 0$. In phase-unbiased topological JJs the system self-tunes into a topological state as the in-plane B is varied by causing a phase jump in $\phi_{\text{GS}} \sim \pi$. We obtain⁵³

$$F(\phi, B) = -k_B T \sum_{E_n, k_y} \ln [2 \cosh(E_n(k_y, B)/2k_B T)], \quad (3)$$

from the calculated spectrum $\{E_n(k_y, B)\}$, where k_B is the Boltzmann constant. The current-phase relation (CPR), $I(\phi, B) = (2e/\hbar) \partial F / \partial \phi$, is then

$$I(\phi, B) = -\frac{e}{\hbar} \sum_{E_n, k_y} \frac{\partial E_n(k_y)}{\partial \phi} \tanh\left(\frac{E_n(k_y, B)}{2k_B T}\right). \quad (4)$$

The extrema of $F(\phi, B)$ corresponds to the zeros of the supercurrent, $I(\phi, B) \propto \partial_\phi F(\phi, B) = 0$, hence ϕ_{GS} follows one of

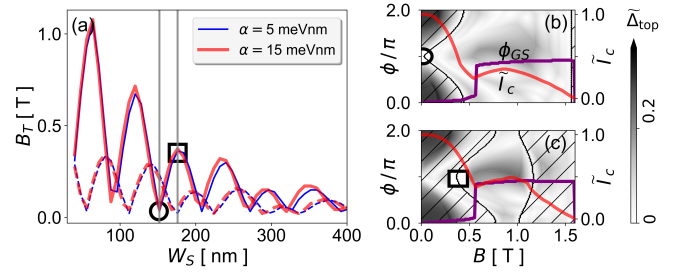


FIG. 2. Finite size effects with $W_N = 160, 600$ nm (solid, dashed) and $\alpha = 5, 15$ meVnm (blue, red). (a) Oscillating minimum topological Zeeman field $B_T(W_S)$ at $\phi = \pi$. (b), (c) Topological phase diagram at a dip, peak in B_T at $W_S = 152, 176$ nm [vertical lines and circle, rectangle in (a)] showing topological charge $Q_D(\phi, B) = 1, -1$ (hatched, unhatched) and normalized topological gap $\Delta_{\text{top}}(\phi, B)$ (grayscale), with superimposed ground state phase $\phi_{\text{GS}}(B)$ (violet, left axis) and normalized critical current $\tilde{I}_c^\pm(B)$ (red, right axis).

the zeros of the CPR.⁵² The forward (reverse) critical current, $I_c^\pm(B)$, is $I_c^\pm(B) = |\min_\phi(\max_\phi) I(\phi, B)|$, and the total critical current is $I_c(B) = \max(I_c^+, I_c^-)$. We normalize critical currents, $\tilde{I}_c(B) \equiv I_c(B)/I_{c,\text{max}}$, $\tilde{I}_c^\pm(B) \equiv I_c^\pm(B)/I_{c,\text{max}}$, to the maximum critical current, $I_{c,\text{max}} \equiv \max_B I_c(B)$. Similarly, $I_{c,\text{min}}$, and $\tilde{I}_{c,\text{min}} \equiv I_{c,\text{min}}/I_{c,\text{max}}$, denote the critical current at its dip near the topological transition and its normalized value.

The class D topological charge, Q_D ,^{13,55-59} for the JJ is

$$Q_D = \text{sgn}[\text{Pf}\{H(k_y = \pi)\sigma_y\tau_y\}/\text{Pf}\{H(k_y = 0)\sigma_y\tau_y\}], \quad (5)$$

where $\text{Pf}\{\dots\}$ denotes the Pfaffian, with $Q_D = 1(-1)$ determining the system in the trivial (topological) phase. We employ experimentally relevant parameters for Al/InAs planar JJs,⁴¹ with $\Delta_0 = 0.23$ meV, $m^* = 0.027m_0$, where m_0 is the bare electron rest mass, and $g^* = 10$. We parametrize the strengths of Rashba and Dresselhaus SOC through an overall strength, λ_{SO} , and an angle, θ_{SO} , defined as

$$\lambda_{\text{SO}} \equiv \sqrt{\alpha^2 + \beta^2}, \quad \theta_{\text{SO}} \equiv \text{arccot}(\alpha/\beta), \quad (6)$$

with $\alpha = \lambda_{\text{SO}} \cos \theta_{\text{SO}}$ and $\beta = \lambda_{\text{SO}} \sin \theta_{\text{SO}}$.^{50,52} We take $\mu(x, y) = \mu_0 - \varepsilon(\lambda_{\text{SO}}, \theta_c)$ constant throughout the system, with $\mu_0 = 1$ meV and $\varepsilon(\lambda_{\text{SO}}, \theta_c) = (2m^* \lambda_{\text{SO}}^2 / \hbar^2) [1 + (\sin 2\theta_c)^2]$ denoting the bottom of the single particle energy band.

The standard model of topological JJs provides important ideas for topological superconductivity and its phase control.¹¹ By assuming Rashba SOC and a perfect transparency, $\tau = 1$,¹¹ at N/S interfaces, which is realized in Al/InAs JJs with $\tau = 0.98$,^{60,61} that model leads to a universal behavior for topological superconductivity. The topological region with $Q_D(\phi, B) = -1$ has a diamond shape,¹¹ formed by closing of a topological gap for $\phi = \pi$, at $B = 0$ and $B^* = \pi\sqrt{2m^*\mu}/(g^*\mu_B W_N)$. For $\phi = 0, 2\pi$ and $Q_D = 1$ at any B , the topological region shrinks to zero. For a phase-unbiased JJ, at $B^*/4$, a topological transition is accompanied by: (i) dip (local minimum) in \tilde{I}_c and (ii) $0 - \pi$ jump in ϕ_{GS} .

With the same assumption of the perfect N/S transparency, in Fig. 2 we find a striking difference from the predicted

universal $B^* \propto 1/W_N$ behavior and a diamond-shape topological region. Finite-size effects in W_S lead to the oscillation of the minimum in-plane Zeeman field for the transition into a topological state, B_T , at $\phi = \pi$, where Q_D switches from 1 to -1 .^{11,59} In Fig. 2(a), for the considered N-region widths, $W_N = 160$ (600) nm, solid (dashed) line, as well as the Rashba SOC strengths, $\alpha = 5$ (15) meVnm, blue (red) line, used throughout our calculations, we see strong oscillations in $B_T(W_S)$. These oscillations also deform the diamond-shaped topological region. This means that, at $\phi = \pi$, a suitable choice of W_S , reducing B_T , can relax the requirements for the onset of topological superconductivity in various materials.

These decaying oscillations in B_T , defined at $\phi = \pi$, are also translated to changes in the whole topological region. For a fixed $W_N = 160$ nm, even a small change in $W_S = 152, 176$ nm [vertical lines mark the corresponding dip and peak in B_T from Fig. 2(a)], leads to a large change in the related size and shape of the topological region in Figs. 2(b) and 2(c), respectively. For example, in Fig. 2(b), we see a topological phase diagram, bounded by a hatched region and $Q_D = 1$. The topological region is large and has a small B_T , even though there is an overall distortion of the diamond shape. However, while the topological region with $Q_D = -1$ implies that MBS can be supported, it is also important to know the corresponding (normalized) topological gap, $\tilde{\Delta}_{\text{top}} \equiv \Delta_{\text{top}}/\Delta_0$, shown as the gray scale background. Specifically, MBS are not well protected in the regions with a small $\Delta_{\text{top}}(\phi, B) \equiv \min(\{E_n(k_y, \phi, B) > 0\})$, where two end-MBS hybridize with each other and move away from zero energy. In contrast, for a slightly wider W_S in Fig. 2(c), we see a much larger B_T and a smaller topological region than in Fig. 2(b).

In previous studies,^{11,30,62} changes from the diamond-shape topological region were attributed to the imperfect transparency which leads to the normal reflection at N/S interfaces, not just Andreev reflections (responsible for the formation of Andreev bound states in JJs). However, even for perfect N/S interfaces, we note that with a finite W_S there are normal reflections at the ends of the S regions. The quasiparticle wavefunctions entering the S regions are reflected back from their ends into the N region and contribute to the normal reflection at the N/S interfaces. The $B_T(W_S)$ oscillations in Fig. 2(a) can be understood from the resonant transmission condition, in which the quasiparticle wavefunction forms a standing wave in the S region.⁵³ This can lead to the transition into the topological phase at a smaller in-plane B and offer a wider topological region for experimentally relevant parameters. The decay of the $B_T(W_S)$ oscillations is consistent with the semiclassical picture of the decaying quasiparticle wavefunction in the S region of width W_S , until it reenters the N region after a travel of $\sim 2W_S$ in the superconductor. With $W_S \rightarrow \infty$, this source of the normal reflection vanishes and thus minimizes B_T .

For chosen parameters in Figs. 2(b) and 2(c), a closer look suggest other deviations from the standard picture. The dip in \tilde{I}_c and $0 - \pi$ jump in ϕ_{GS} no longer take place at the same value of B , which can be much more pronounced in other cases.^{41,52} The jump in ϕ_{GS} is generally different from π ,⁶³ the size of the jump decreases with α . Together, this suggests that, even for a perfect N/S transparency, there is a considerably richer

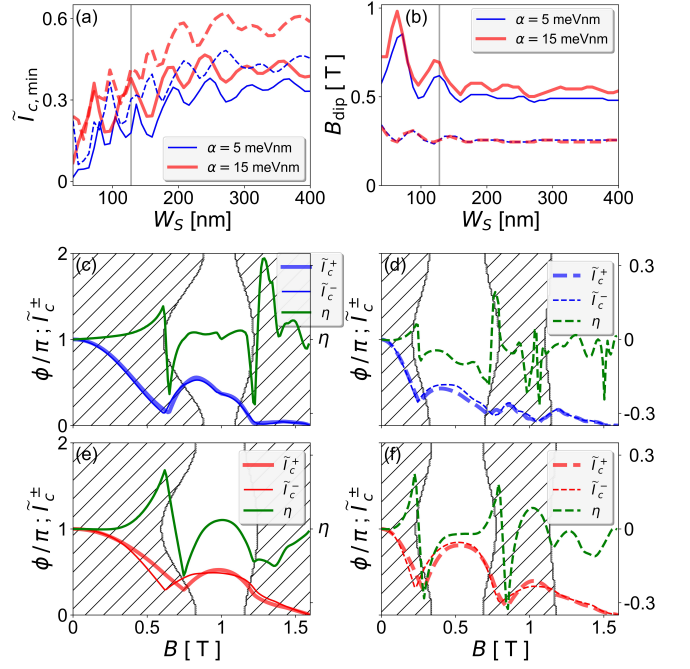


FIG. 3. Critical current dip near the first topological transition and superconducting diode effect; solid/dashed lines and colors follow the convention introduced in Fig. 2 for W_N and α . (a) Oscillating critical current at dip, $\tilde{I}_{c,\text{min}}(W_S)$. (b) Zeeman field at dip, $B_{\text{dip}}(W_S)$. (c) - (f) Diode effect for $W_S = 128$ nm [gray line in (a), (b)]: unequal forward, reverse normalized critical current $\tilde{I}_c^\pm(B)$ (thick, thin line; left axis), diode effect efficiency $\eta(B)$ for $\alpha = 15$ meVnm (green, right axis), and topological charge $Q_D = 1, -1$ (hatched, unhatched).

behavior for topological JJs than commonly expected, warranting our further analysis and identifying opportunities to facilitate experimental implementation of JJs.

With this motivation, we next investigate the size and location of the dip of \tilde{I}_c , denoted by $\tilde{I}_{c,\text{min}}$ and B_{dip} , respectively, and shown in Figs. 3(a) and 3(b). This dip corresponds to the minimization of the singlet component of the finite-momentum wavefunction, which vanishes near the topological phase transition in the absence of normal reflection in the JJ.^{11,47,50,52} At a fixed temperature, the magnitude of \tilde{I}_c is thus related to the contribution of the normal reflection. Therefore, oscillations in $\tilde{I}_c(W_S)$, similar to those in Fig. 2(a), are also present in Fig. 3(a). However, unlike only a weak dependence of the magnitude of $B_T(W_S)$ oscillations with α in Fig. 2(a), the same change in the Rashba SOC strongly changes the magnitude of the $\tilde{I}_c(W_S)$ in Figs. 3(a), for both $W_N = 160$ and 600 nm. Turning to the dip location in Fig. 3(b), $B_{\text{dip}}(W_S)$ shows decaying oscillations which are strongly suppressed for a larger W_N and with increasing W_S . Since a finite W_S changes the shape of the topological region and $Q_D(\phi, B) = -1$, various predicted universal features of the standard planar JJ model no longer hold. By comparing Figs. 3(b) and 3(c), we see that, even at $\phi = \pi$, the location of the dip is outside of the topological region. Furthermore, this location does not coincide with that of the phase jump, nor with the location for the

transition of the phase-unbiased system into the topological region,⁴¹ as seen in Figs. 2(b) and 2(c), red line.

With the recently renewed interest in nonreciprocal transport and diode effects in superconducting junctions,^{2,46} we note that the 2019 report of the phase signature of the transition to topological superconductivity in planar JJs was also accompanied by the measured superconducting diode effect,^{2,41} but was not discussed. The diode effect, while not considered in the standard model of planar JJs, is also inherent to these systems.⁶⁴ We parametrize the efficiency of the diode effect by the asymmetry of the critical currents⁶⁵

$$\eta \equiv (I_c^+ - I_c^-) / (I_c^+ + I_c^-), \quad (7)$$

shown along with the forward and reverse \tilde{I}_c^\pm for $W_S = 128$ nm in Figs. 3(c), 3(d) for $W_N = 160$ nm, and in Figs. 3(e)-3(f). Red/blue curves retain our convention for $\alpha = 5, 15$ eVnm. An observed trend here, that \tilde{I}_c^+ and \tilde{I}_c^- will differ more for a larger α and larger W_N , is expected from the spin-dependent phase shift of electron and hole forming the Andreev bound states.⁶⁴ Away from the dip locations of \tilde{I}_c^\pm , $\eta \sim 0.1$, while near the \tilde{I}_c^\pm η becomes much larger, but also accompanied with only a small I_c .^{47,52} The sign change locations in η correspond to either the minimized singlet or the triplet part of the finite-momentum pairing wavefunctions, which occur at different locations for narrow and wide JJs.⁴⁷ These finite-size effects could guide future experiments on both superconducting diode effect and topological phase transitions in JJs.

Most of the work on topological JJs considered only Rashba SOC. While for certain crystallographic directions the spin texture from Dresselhaus SOC⁴⁸ recovers the one expected from only Rashba SOC in Eq. (2), with the simultaneous presence of these two SOC contributions, present in many 2DEGs, the topological phase diagram can be strongly modified. In a situation from Fig. 1, where in-plane \mathbf{B} is perpendicular to the current direction and for a narrow JJ with $\beta \neq 0$, one can find that Δ_{top} together with MBS protection are maximized for $\theta_c = \pi/4$ for an arbitrary ratio α/β , i.e. an arbitrary θ_{SO} ,⁵⁰⁻⁵² recall Eq. (6). We thus limit our results to $\theta_c = \pi/4$ and consider the cases where Rashba and Dresselhaus have equal strengths, $\theta_{\text{SO}} = \pi/4$, or the system has only Dresselhaus SOC, $\theta_{\text{SO}} = \pi/2$, while keeping constant the combined SOC magnitude, λ_{SO} , defined in Eq. (6).

To consider the influence of Dresselhaus SOC, in Figs. 4(a) and (b), we first revisit the oscillation of the topological transition field, $B_T(W_S)$, shown previously in Fig. 2(a) for $\beta = 0$. By choosing $\lambda_{\text{SO}} = 15$ meVnm in Fig. 4, we have a direct comparison with the red curves for $\alpha = 15$ meVnm from Fig. 2 which show very similar decaying oscillations with W_S , while the results from Figs. 4(a) and (b) again confirm that amplitude of these oscillations is suppressed with W_N . We also see that, it is not only the combined SOC magnitude, but also the relative contribution of Dresselhaus and Rashba SOC which determines the oscillations in $B_T(W_S)$, shifted to the right for a larger β ($\theta_{\text{SO}} = \pi/2$) that becomes more pronounced with a wider W_N . As a result, while the oscillating trends in $B_T(W_S)$ are retained without and with Dresselhaus SOC, at a given W_S and W_N , a change in the relative strength of

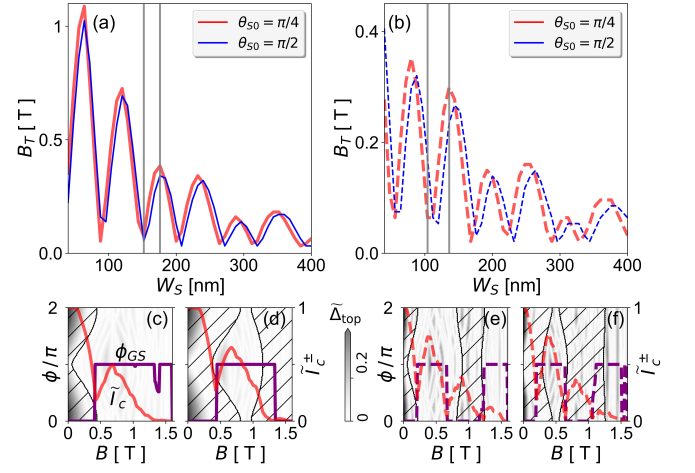


FIG. 4. Effects of Dresselhaus SOC; in all plots $\lambda_{\text{SO}} = \sqrt{\alpha^2 + \beta^2} = 15$ meVnm and $\theta_c = \pi/4$, see Eq. (2). Solid/dashed lines indicate W_N as in Figs. 2, 3. (a), (b) Oscillating $B_T(W_S)$; $\theta_{\text{SO}} = \pi/4$ (red) [$\pi/2$, blue] corresponds to $\alpha = \beta$ ($\alpha = 0$). (c)-(f) Topological phase diagrams with $Q_D(\phi, B) = 1, -1$ (hatched, unhatched) and $\Delta_{\text{top}}(\phi, B)$ (grayscale), with $\phi_{\text{GS}}(B)$ (violet, right axis) and $\tilde{I}_c(B)$ (red, left axis). (c), (d) correspond to a minimum, peak in $B_T(W_S)$ at $W_S = 152, 176$ nm [gray lines in (a)]. (e), (f) correspond to a minimum, peak at $W_S = 104, 136$ nm [gray lines in (b)].

the Rashba and Dresselhaus SOC strongly alter the value of B_T and thus also the topological phase diagram. For example, at $W_S = 104$ nm, in Figs. 2(a) and 4(b) we can compare the three corresponding B_T values with the same SOC strength $\lambda_{\text{SO}} = 15$ meVnm, but with various relative strengths of the Dresselhaus SOC. Using a pure Dresselhaus SOC as a reference, B_T for a mixed Rashba and Dresselhaus SOC in Fig. 4(b) differ by ~ 0.1 T, while for a pure Rashba SOC in Fig. 2(a), the difference in is ~ 0.08 T. Correspondingly, with a change in the relative strength of Rashba and Dresselhaus SOC, the topological phase diagram and the onset of topological superconductivity can be noticeably different.

Another influence of Dresselhaus SOC can be seen in Fig. 4(c) and 4(d) for the two chosen values of W_S , marked by gray lines in Figs. 4(a) and 4(b) and matching the W_S values in Fig. 2. Several differences from $\beta = 0$ and Figs. 2(b) and 2(c) can be inferred, where the evolution of \tilde{I}_c with B was overall smoother and the jumps in ϕ_{GS} were less abrupt than seen in Fig. 4(c) and 4(d). This is consistent with a shallower landscape for the free energy when $\beta \neq 0$, which supports more rapid changes with B , including the dip in the ϕ_{GS} in Fig. 4(c). We note that the choice of \mathbf{B} along the y axis in Fig. 1(a) maximized $\Delta_{\text{top}}(\phi, B)$ for $\beta = 0$ and led to its reduction in Fig. 4(c)-4(f). With a larger $W_N = 600$ nm in Figs. 4(e) and 4(f), there are even more abrupt changes in \tilde{I}_c and ϕ_{GS} . While not shown in Fig. 4, $\beta \neq 0$ again supports the superconducting diode effect, discussed in Fig. 3.

Planar JJs provide a versatile platform for topological superconductivity as well as for superconducting spintronics,⁶⁶⁻⁶⁸ through spin-triplet supercurrents and superconducting diode effect.^{2,46,69} Even for a perfect inter-

facial transparency, we find a much richer behavior than what is expected from the common description of planar JJs. There are interesting future generalizations where our results could offer a helpful starting point. For example, in exploring the role of disorder in planar JJs,^{70,71} or more complex geometries,^{37,72,73} it is important to include the relevant form of SOC and the finite-size effects. With a growing class of materials used in JJs, SOC that is linear in the wave vector may not be sufficient and the cubic SOC terms could become dominant.^{74–77} As a result, instead of the spin-triplet p -wave, the proximity-induced topological superconductivity could acquire the character of the spin-triplet f -wave.⁷⁵

The data that support the findings of this study are available from the corresponding author upon reasonable request.

ACKNOWLEDGMENTS

This work is supported by US ONR under awards MURI N000142212764, N000141712793, and NSF ECCS-2130845. Computational resources were provided by the UB Center for Computational Research.

- ¹Žutić, I., A. Matos-Abiague, B. Scharf, H. Dery, and K. Belashchenko, “Proximitized materials,” *Mater. Today* **22**, 85 (2019).
- ²M. Amundsen, J. Linder, J. W. A. Robinson, I. Žutić, and N. Banerjee, “Colloquium: Spin-orbit effects in superconducting hybrid structures,” *Rev. Mod. Phys.* **96**, 021003 (2024).
- ³F. Tafuri (ed.), *Fundamentals and Frontiers of the Josephson Effect* (Springer Nature, Cham, 2019).
- ⁴B. D. Josephson, “Possible new effects in superconductive tunnelling,” *Phys. Lett.* **1**, 251 (1962).
- ⁵R. Holm and W. Meissner, “Messungen mit hilfe von flüssigem helium. XIII,” *Z. Phys.* **74**, 75 (1932).
- ⁶L. Fu and C. L. Kane, “Superconducting proximity effect and Majorana fermions at the surface of a topological insulator,” *Phys. Rev. Lett.* **100**, 096407 (2008).
- ⁷A. Keselman, L. Fu, A. Stern, and E. Berg, “Inducing time-reversal-invariant topological superconductivity and fermion parity pumping in quantum wires,” *Phys. Rev. Lett.* **111**, 116402 (2013).
- ⁸B. van Heck, S. Mi, and A. R. Akhmerov, “Single fermion manipulation via superconducting phase differences in multiterminal Josephson junctions,” *Phys. Rev. B* **90**, 155450 (2014).
- ⁹P. Kotetes, “Topological superconductivity in Rashba semiconductors without a Zeeman field,” *Phys. Rev. B* **92**, 014514 (2015); [Erratum: Topological superconductivity in Rashba semiconductors without a Zeeman field,” *Phys. Rev. B* **101**, 209904 (2020)].
- ¹⁰M. Hell, M. Leijnse, and K. Flensberg, “Two-dimensional platform for networks of Majorana bound states,” *Phys. Rev. Lett.* **118**, 107701 (2017).
- ¹¹F. Pientka, A. Keselman, E. Berg, A. Yacoby, A. Stern, and B. I. Halperin, “Topological superconductivity in a planar Josephson junction,” *Phys. Rev. X* **7**, 021032 (2017).
- ¹²T. Zhou, M. C. Dartiailh, W. Mayer, J. E. Han, A. Matos-Abiague, J. Shabani, and I. Žutić, “Phase control of Majorana bound states in a topological X junction,” *Phys. Rev. Lett.* **124**, 137001 (2020).
- ¹³A. Y. Kitaev, “Unpaired Majorana fermions in quantum wires,” *Phys.-Usp.* **44**, 131 (2001).
- ¹⁴A. Kitaev, “Fault-tolerant quantum computation by anyons,” *Ann. Phys.* **303**, 2 (2003).
- ¹⁵R. M. Lutchyn, J. D. Sau, and S. Das Sarma, “Majorana fermions and a topological phase transition in semiconductor-superconductor heterostructures,” *Phys. Rev. Lett.* **105**, 077001 (2010).
- ¹⁶Y. Oreg, G. Refael, and F. von Oppen, “Helical liquids and Majorana bound states in quantum wires,” *Phys. Rev. Lett.* **105**, 177002 (2010).
- ¹⁷L. P. Rokhinson, X. Liu, and J. K. Furdyna, “The fractional a.c. Josephson effect in a semiconductor-superconductor nanowire as a signature of Majorana particles,” *Nat. Phys.* **8**, 795 (2012).
- ¹⁸M. Leijnse and K. Flensberg, “Introduction to topological superconductivity and Majorana fermions,” *Semicond. Sci. Technol.* **27**, 124003 (2012).
- ¹⁹D. Aasen, M. Hell, R. V. Mishmash, A. Higginbotham, J. Danon, M. Leijnse, T. S. Jespersen, J. A. Folk, C. M. Marcus, K. Flensberg, and J. Alicea, “Milestones toward Majorana-based quantum computing,” *Phys. Rev. X* **6**, 031016 (2016).
- ²⁰K. Laubscher and J. Klinovaja, “Majorana bound states in semiconducting nanostructures,” *J. Appl. Phys.* **130**, 081101 (2021).
- ²¹P. Marra, “Majorana nanowires for topological quantum computation,” *J. Appl. Phys.* **132**, 231101 (2022).
- ²²K. Sengupta, I. Žutić, H.-J. Kwon, V. M. Yakovenko, and S. Das Sarma, “Midgap edge states and pairing symmetry of quasi-one-dimensional organic superconductors,” *Phys. Rev. B* **63**, 144531 (2001).
- ²³V. Mourik, K. Zuo, S. M. Frolov, S. R. Plissard, E. P. A. M. Bakkers, and L. P. Kouwenhoven, “Signatures of Majorana fermions in hybrid superconductor-semiconductor nanowire devices,” *Science* **336**, 1003 (2012).
- ²⁴E. J. H. Lee, X. Jiang, R. Aguado, G. Katsaros, C. M. Lieber, and S. De Franceschi, “Zero-bias anomaly in a nanowire quantum dot coupled to superconductors,” *Phys. Rev. Lett.* **109**, 186802 (2012).
- ²⁵A. Das, Y. Ronen, Y. Most, Y. Oreg, M. Heiblum, and H. Shtrikman, “Zero-bias peaks and splitting in an Al-InAs nanowire topological superconductor as a signature of Majorana fermions,” *Nat. Phys.* **8**, 887 (2012).
- ²⁶J. Chen, B. D. Woods, P. Yu, M. Hocevar, D. Car, S. R. Plissard, E. P. A. M. Bakkers, T. D. Stanescu, and S. M. Frolov, “Ubiquitous non-Majorana zero-bias conductance peaks in nanowire devices,” *Phys. Rev. Lett.* **123**, 107703 (2019).
- ²⁷S. Das Sarma and H. Pan, “Disorder-induced zero-bias peaks in Majorana nanowires,” *Phys. Rev. B* **103**, 195158 (2021).
- ²⁸P. Yu, J. Chen, M. Gomanko, G. Badawy, E. P. A. M. Bakkers, K. Zuo, V. Mourik, and S. M. Frolov, “Non-Majorana states yield nearly quantized conductance in proximitized nanowires,” *Nat. Phys.* **17**, 482 (2021).
- ²⁹J. Shabani, M. Kjaergaard, H. J. Suominen, Y. Kim, F. Nichele, K. Pakrouski, T. Stankevici, R. M. Lutchyn, P. Krogstrup, R. Feidenhans’l, S. Kraemer, C. Nayak, M. Troyer, C. M. Marcus, and C. J. Palmström, “Two-dimensional epitaxial superconductor-semiconductor heterostructures: A platform for topological superconducting networks,” *Phys. Rev. B* **93**, 155402 (2016).
- ³⁰B. Scharf, F. Pientka, H. Ren, A. Yacoby, and E. Hankiewicz, “Tuning topological superconductivity in phase-controlled Josephson junctions with Rashba and Dresselhaus spin-orbit coupling,” *Phys. Rev. B* **99**, 214503 (2019).
- ³¹P. Virtanen, F. S. Bergeret, E. Strambini, F. Giazotto, and A. Braggio, “Majorana bound states in hybrid two-dimensional Josephson junctions with ferromagnetic insulators,” *Phys. Rev. B* **98**, 020501(R) (2018).
- ³²T. Zhou, M. C. Dartiailh, K. Sardashti, J. E. Han, A. Matos-Abiague, J. Shabani, and I. Žutić, “Fusion of Majorana bound states with mini-gate control in two-dimensional systems,” *Nat. Commun.* **13**, 1738 (2022).
- ³³F. Setiawan, C.-T. Wu, and K. Levin, “Full proximity treatment of topological superconductors in Josephson-junction architectures,” *Phys. Rev. B* **99**, 174511 (2019).
- ³⁴G. L. Fatin, A. Matos-Abiague, B. Scharf, and I. Žutić, “Wireless Majorana bound states: From magnetic tunability to braiding,” *Phys. Rev. Lett.* **117**, 077002 (2016).
- ³⁵A. Matos-Abiague, J. Shabani, A. D. Kent, G. L. Fatin, B. Scharf, and I. Žutić, “Tunable magnetic textures: From Majorana bound states to braiding,” *Solid State Commun.* **262**, 1 (2017).
- ³⁶P. P. Paudel, T. Cole, B. D. Woods, and T. D. Stanescu, “Enhanced topological superconductivity in spatially modulated planar Josephson junctions,” *Phys. Rev. B* **104**, 155428 (2021).
- ³⁷N. Pankratova, H. Lee, R. Kuzmin, K. Wickramasinghe, W. Mayer, J. Yuan, M. G. Vavilov, J. Shabani, and V. E. Manucharyan, “Multiterminal Josephson effect,” *Phys. Rev. X* **10**, 031051 (2020).
- ³⁸U. Güngördü and A. A. Kovalev, “Majorana bound states with chiral magnetic textures,” *J. Appl. Phys.* **132**, 041101 (2022).
- ³⁹A. Fornieri, A. M. Whiticar, F. Setiawan, E. Portolés, A. C. C. Drachmann, A. Keselman, S. Gronin, C. Thomas, T. Wang, R. Kallaher, G. C.

- Gardner, E. Berg, M. J. Manfra, A. Stern, C. M. Marcus, and F. Nichele, "Evidence of topological superconductivity in planar Josephson junctions," *Nature* **569**, 89 (2019).
- ⁴⁰H. Ren, F. Pientka, S. Hart, A. Pierce, M. Kosowsky, L. Lunczer, R. Schlereth, B. Scharf, E. M. Hankiewicz, L. W. Molenkamp, B. I. Halperin, and A. Yacoby, "Topological superconductivity in a phase-controlled Josephson junction," *Nature* **569**, 93 (2019).
- ⁴¹M. C. Dartiaillh, W. Mayer, J. Yuan, K. S. Wickramasinghe, A. Matos-Abiague, I. Žutić, and J. Shabani, "Phase signature of topological transition in Josephson junctions," *Phys. Rev. Lett.* **126**, 036802 (2021), arXiv:1906.0117.
- ⁴²A. Banerjee, O. Lesser, M. A. Rahman, H.-R. Wang, M.-R. Li, A. Kringshøj, A. M. Whiticar, A. C. C. Drachmann, C. Thomas, T. Wang, M. J. Manfra, E. Berg, Y. Oreg, A. Stern, and C. M. Marcus, "Signatures of a topological phase transition in a planar Josephson junction," *Phys. Rev. B* **107**, 245304 (2023).
- ⁴³A. Banerjee, M. Geier, M. A. Rahman, D. S. Sanchez, C. Thomas, T. Wang, M. J. Manfra, K. Flensberg, and C. M. Marcus, "Control of Andreev bound states using superconducting phase texture," *Phys. Rev. Lett.* **130**, 116203 (2023).
- ⁴⁴R. Li, W. Song, W. Miao, Z. Yu, Z. Wang, S. Yang, Y. Gao, Y. Wang, F. Chen, Z. Geng, L. Yang, J. Xu, X. Feng, T. Wang, Y. Zang, L. Li, R. Shang, Q. Xue, K. He, and H. Zhang, "Selective-area-grown PbTe-Pb planar Josephson junctions for quantum devices," *Nano Lett.* **24**, 4658 (2024).
- ⁴⁵C. Baumgartner, L. Fuchs, A. Costa, S. Reinhardt, S. Gronin, G. C. Gardner, T. Lindemann, M. J. Manfra, P. E. F. Junior, D. Kochan, J. Fabian, N. Paradiso, and C. Strunk, "Supercurrent rectification and magnetochiral effects in symmetric Josephson junctions," *Nat. Nanotechnol.* **17**, 39 (2022).
- ⁴⁶M. Nadeem, M. S. Fuhrer, and X. Wang, "The superconducting diode effect," *Nat. Rev. Phys.* **5**, 558 (2023).
- ⁴⁷N. Lotfizadeh, W. Schiela, B. Pekerten, P. Yu, W. Strickland, A. Matos-Abiague, and J. Shabani, "Superconducting diode effect sign change in epitaxial Al-InAs Josephson junctions," *Commun. Phys.* **7**, 120 (2024).
- ⁴⁸I. Žutić, J. Fabian, and S. Das Sarma, "Spintronics: Fundamentals and applications," *Rev. Mod. Phys.* **76**, 323 (2004).
- ⁴⁹J. Fabian, A. Matos-Abiague, C. Ertler, P. Stano, and I. Žutić, "Semiconductor spintronics," *Acta Phys. Slov.* **57**, 565 (2007).
- ⁵⁰J. Pakizer, B. Scharf, and A. Matos-Abiague, "Crystalline anisotropic topological superconductivity in planar Josephson junctions," *Phys. Rev. Res.* **3**, 013198 (2021).
- ⁵¹J. Pakizer and A. Matos-Abiague, "Signatures of topological transitions in the spin susceptibility of Josephson junctions," *Phys. Rev. B* **104**, L100506 (2021).
- ⁵²B. Pekerten, J. D. Pakizer, B. Hawn, and A. Matos-Abiague, "Anisotropic topological superconductivity in Josephson junctions," *Phys. Rev. B* **105**, 054504 (2022).
- ⁵³M. Tinkham, *Introduction to Superconductivity* (McGraw-Hill, New York, 1996).
- ⁵⁴C. W. Groth, A. R. Akhmerov, and X. Waintal, "Kwant: a software package for quantum transport," *New J. Phys.* **16**, 063065 (2014).
- ⁵⁵A. Altland and M. Zirnbauer, "Nonstandard symmetry classes in mesoscopic normal-superconducting hybrid structures," *Phys. Rev. B* **55**, 1142 (1997).
- ⁵⁶A. Schnyder, S. Ryu, A. Furusaki, A. Ludwig, V. Lebedev, and M. Feigel'man, "Classification of topological insulators and superconductors," *AIP Conf. Proc.* **1134**, 10 (2009).
- ⁵⁷S. Ryu, A. Schnyder, A. Furusaki, and A. Ludwig, "Topological insulators and superconductors: tenfold way and dimensional hierarchy," *New J. Phys.* **12**, 065010 (2010).
- ⁵⁸P. Ghosh, J. Sau, S. Tewari, and S. Das Sarma, "Non-abelian topological order in noncentrosymmetric superconductors with broken time-reversal symmetry," *Phys. Rev. B* **82**, 184525 (2010).
- ⁵⁹S. Tewari and J. D. Sau, "Topological invariants for spin-orbit coupled superconductor nanowires," *Phys. Rev. Lett.* **109**, 150408 (2012).
- ⁶⁰M. Kjaergaard, H. Suominen, M. Nowak, A. Akhmerov, J. Shabani, C. J. Palmström, F. Nichele, and C. Marcus, "Transparent semiconductor-superconductor interface and induced gap in an epitaxial heterostructure Josephson junction," *Phys. Rev. Applied* **7**, 034029 (2017).
- ⁶¹F. Nichele, E. Portolés, A. Fornieri, A. M. Whiticar, A. C. C. Drachmann, S. Gronin, T. Wang, G. C. Gardner, C. Thomas, A. Hatke, M. J. Manfra, and C. M. Marcus, "Relating Andreev bound states and supercurrents in hybrid Josephson junctions," *Phys. Rev. Lett.* **124**, 226801 (2020).
- ⁶²F. Setiawan, A. Stern, and E. Berg, "Topological superconductivity in planar Josephson junctions: Narrowing down to the nanowire limit," *Phys. Rev. B* **99**, 220506 (2019).
- ⁶³B. Pekerten, A. C. Prasannan, B. Scharf, and A. Matos-Abiague, "Topological superconductivity and Josephson diode effects on the magnetocurrent-phase relation of planar Josephson junctions," preprint (2024).
- ⁶⁴T. Yokoyama, M. Eto, and Y. V. Nazarov, "Anomalous Josephson effect induced by spin-orbit interaction and Zeeman effect in semiconductor nanowires," *Phys. Rev. B* **89**, 195407 (2014).
- ⁶⁵Y. Hou, F. Nichele, H. Chi, A. Lodesani, Y. Wu, M. F. Ritter, D. Z. Haxell, M. Davydova, S. Ilić, O. Glezakou-Elbert, A. Varambally, F. S. Bergeret, A. Kamra, L. Fu, P. A. Lee, and J. S. Moodera, "Ubiquitous superconducting diode effect in superconductor thin films," *Phys. Rev. Lett.* **131**, 027001 (2023).
- ⁶⁶J. Linder and J. W. A. Robinson, "Superconducting spintronics," *Nat. Phys.* **11**, 307 (2015).
- ⁶⁷M. Eschrig, "Spin-polarized supercurrents for spintronics: A review of current progress," *Rep. Prog. Phys.* **78**, 104501 (2015).
- ⁶⁸R. Cai, I. Žutić, and W. Han, "Superconductor/ferromagnet heterostructures: A platform for superconducting spintronics and quantum computation," *Adv. Quantum Technol.* **6**, 2200080 (2023).
- ⁶⁹N. Banerjee, J. W. A. Robinson, and M. G. Blamire, "Reversible control of spin-polarized supercurrents in ferromagnetic Josephson junctions," *Nat. Commun.* **5**, 4771 (2014).
- ⁷⁰A. Stern and E. Berg, "Fractional Josephson vortices and braiding of Majorana zero modes in planar superconductor-semiconductor heterostructures," *Phys. Rev. Lett.* **122**, 107701 (2019).
- ⁷¹V. D. Kurilovich, Z. M. Raines, and L. I. Glazman, "Disorder-enabled Andreev reflection of a quantum Hall edge," *Nat. Commun.* **14**, 2237 (2023).
- ⁷²P. Kotetes, M. T. Mercaldo, and M. Cuoco, "Synthetic Weyl points and chiral anomaly in Majorana devices with nonstandard Andreev-bound-state spectra," *Phys. Rev. Lett.* **123**, 126802 (2019).
- ⁷³T. W. Schmitt, M. R. Connolly, M. Schleenvoigt, C. Liu, O. Kennedy, J. M. Chávez-García, A. R. Jalil, B. Bennemann, S. Trellenkamp, F. Lentz, E. Neumann, T. Lindström, S. E. de Graaf, E. Berenschoot, N. Tas, G. Müsler, K. D. Petersson, D. Grützmacher, and P. Schüffelgen, "Integration of topological insulator Josephson junctions in superconducting qubit circuits," *Nano Lett.* **22**, 2595 (2022).
- ⁷⁴K. V. Samokhin, "On the effective models of spin-orbit coupling in a two-dimensional electron gas," *Ann. Phys.* **437**, 168710 (2022).
- ⁷⁵M. Alidoust, C. Shen, and I. Žutić, "Cubic spin-orbit coupling and anomalous Josephson effect in planar junctions," *Phys. Rev. B* **103**, L060503 (2021).
- ⁷⁶M. Luethi, K. Laubscher, S. Bosco, D. Loss, and J. Klinovaja, "Planar Josephson junctions in germanium: Effect of cubic spin-orbit interaction," *Phys. Rev. B* **107**, 035435 (2023).
- ⁷⁷A. A. Tosato, V. Levajac, J.-Y. Wang, C. J. Boor, F. Borsoi, M. B. C. N. Borja, S. Marti-Sanchez, J. Arbiol, A. Sammak, M. Veldhorst, and G. Scappucci, "Hard superconducting gap in a high-mobility semiconductor," *Commun. Mater.* **4**, 23 (2023).